Synthetic and Systems Biotechnology 10 (2025) 271–280

Contents lists available at ScienceDirect

Synthetic and Systems Biotechnology

journal homepage: www.keaipublishing.com/en/journals/synthetic-and-systems-biotechnology

Original Research Article

De novo synthesis of 1-phenethylisoquinoline in engineered *Escherichia coli*

Yaping Mao [a,b,c,1], Jiangming Zhu [a,b,c,1], Qian Zhang [a,b], Guangyi Wang [a,b], Hongkai Fan [a,b], Xiaowei Zhang [a], Yuwei Sun [a,*], Yong Wang [a,b,c,**]

[a] CAS-Key Laboratory of Synthetic Biology, CAS Center for Excellence in Molecular Plant Sciences, Chinese Academy of Sciences, Shanghai 200032, China
[b] University of Chinese Academy of Sciences, Beijing 100039, China
[c] State Key Laboratory of Bioreactor Engineering, East China University of Science and Technology, Shanghai 200237, China

ARTICLE INFO

Keywords:
Phenylethylisoquinoline alkaloids
1-Phenethylisoquinoline
De novo biosynthesis
Escherichia coli
Reductases

ABSTRACT

Phenylethylisoquinoline alkaloids (PIAs) are medicinally important natural products derived from the 1-phenylethylisoquinoline precursor. Heterologous production of the PIAs remains challenging due to the incomplete elucidation of biosynthetic pathway and the lack of proper microbial cell factory designed for precursor enhancement. In this work, an artificial pathway composed of eight enzymes from different species was established for de novo 1-phenylethylisoquinoline biosynthesis in engineered *Escherichia coli*. The yield of the intermediate 4-hydroxydihydrocinnamaldehyde was optimized through screening various $NADP^+$-dependent 2-alkenal reductases, cofactor regeneration and the site-directed mutagenesis of key residues in ChAER1. Subsequently, incorporation of the modified dopamine pathway into an endogenous reductase-deficient *E. coli* with high tyrosine yield boosted the production of 1-phenylethylisoquinoline, reaching 402.58 mg/L in a 5L fermenter. Our work lays a foundation for the future large-scale production of high value-added 1-phenylethylisoquinoline-related alkaloids.

1. Introduction

Isoquinoline alkaloids are medicinally important phytochemicals, which form the largest class (>3000) of naturally occurring alkaloid products [1]. According to different core substructures, the isoquinoline alkaloids can be mainly classified into simple isoquinolines, benzylisoquinoline alkaloids (BIAs), phenylethylisoquinoline alkaloids (PIAs), etc [2,3]. PIA metabolites have attracted widespread attention due to their intriguing bioactivities. Among them, the most prominent examples are homoharringtonine from plum yews (*Cephalotaxus*), colchicine from flame lily (*Gloriosa*), and melanthioidine from African crocus (*Androcymbium*) (Fig. 1). Homoharringtonine was the only commercially available medication approved by the U.S. Food & Drug Administration (FDA) in 2012 for the treatment of acute chronic myelogenous leukemia [4–6] while colchicine have also been approved by the FDA to treat acute gout, familial Mediterranean fever and pericarditis and Behçet's disease [7,8]. Currently, the PIA-based preparations or medicines are mainly produced by extracting the *Cephalotaxus* and *Colchicum* plants, which heavily rely on the wild resources and cultivation [9]. Alternatively, several chemical synthesis approaches have been developed to meet the needs of clinical research and treatment [10–12], nevertheless the lengthy synthetic route resulted in low yields that was not sufficient for large-scale application. On the other hand, with the development of synthetic biology approaches, microbial biosynthesis has been playing important role in providing new solution to limited sources of drug molecules. Significant breakthroughs have been made in alkaloids production, such as the de novo synthesis of BIA in engineered microbial chassis like *Escherichia coli* and *Saccharomyces cerevisiae* [13–18].

In contrast to the well-studied BIA biosynthesis, the PIA biosynthetic pathways remain largely unknown till very recent achievement on the elucidation of colchicine and homoharringtonine biogenesis (Fig. 1A). A set of newly discovered tailoring enzymes (i.e., cytochrome P450 monooxygenases, *O*- and *N*-methyltransferases) have been reported to generate *N*-formyldemecolcine from 1-phenylethylisoquinoline (**1**), a

Peer review under responsibility of KeAi Communications Co., Ltd.
* Corresponding author.
** Corresponding author. CAS-Key Laboratory of Synthetic Biology, CAS Center for Excellence in Molecular Plant Sciences, Chinese Academy of Sciences, Shanghai 200032, China.
E-mail addresses: ywsun@cemps.ac.cn (Y. Sun), yongwang@cemps.ac.cn (Y. Wang).
[1] These authors contributed equally.

https://doi.org/10.1016/j.synbio.2024.10.007
Received 17 August 2024; Received in revised form 19 October 2024; Accepted 30 October 2024
Available online 9 November 2024

common precursor of all PIA compounds [19]. However, the pathway leading to **1** remained elusive until ChPSS (a new member of the pathogenesis-related 10/Bet v1 family), along with ChDBR (NADPH--dependent double-bond reductases), were identified as key enzymes responsible for producing **1** in *Cephalotaxus hainanensis* [9]. It has become clear that the **1** scaffold plays a central role in the biosynthesis of all PIAs, and this nucleus is derived from both L-phenylalanine and L-tyrosine (Fig. 1). L-Tyrosine is first catalyzed by tyrosinase (TYR) or tyrosine hydroxylase (TyrH) to produce L-DOPA (**2**), which is then decarboxylated to dopamine (**3**). Alternatively, decarboxylation of tyrosine produce tyramine as an intermediate ready to be hydroxylated to **3**. On the other hand, L-phenylalanine is deaminated by phenylalanine ammonia-lyase (PAL) to produce cinnamic acid, which then undergoes successive oxidoreduction by cinnamic acid-4-hydroxylase (C4H), 4-coumarate-CoA ligase (4CL), cinnamoyl-CoA reductase (CCR), and NADPH-dependent 2-alkenal reductase (AER) (also known as DBR) to the final product 4-hydroxydihydrocinnamaldehyde (4-HDCA, **4**). Finally, the tyrosine-derived **3** and phenylalanine-derived **4** were linked by the Pictet–Spenglerase (PSS)-mediated condensation to form the **1** backbone (Fig. 1). The formation of **4** by AER-mediated hydrogenation of 4-coumaraldehyde is a crucial step for the initiation of downstream biosynthesis in the specialized PIAs pathway, since the α,β-double bond reduction of the aldehyde moiety is absent in the common metabolism of other shikimate pathway-derived natural products, such as BIAs, flavonoids, coumarin, etc. Nevertheless, similar double-bond reduction occurs in the biosynthesis of dihydrophenylpropane derivatives, which may contribute to heartwood formation and defence against insects [20].

The first attempt of heterologous production of **1** has been reported in the work of colchicine pathway discovery, in which the researchers applied 16 newly identified enzymes to build a biosynthetic route from phenylalanine/tyrosine to *N*-formyldemecolcine in *Nicotiana benthamiana* [19] (Fig. 1B). According the results reported by Sattely and co-workers, joining the **3** and **4** pathway by (*S*)-norcoclurine synthases from *Coptis japonica* (CjNCS) gave **1**, while its yield was not mentioned. Instead of in situ production of the aldehyde intermediate **4**, Zhang et al.

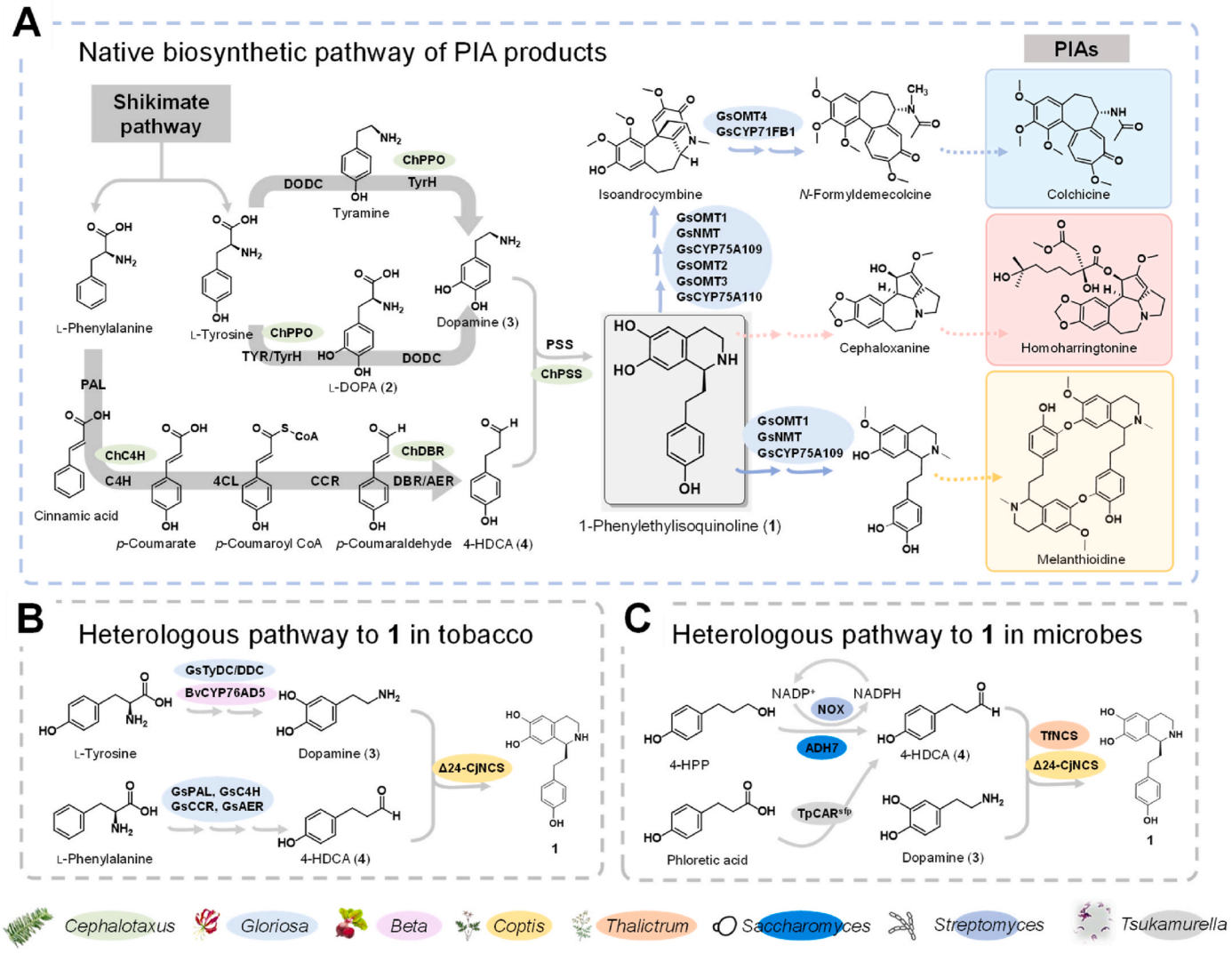

Fig. 1. Biosynthetic pathway of 1-phenylethylisoquinoline-derived PIAs. (A) Native biosynthetic route of PIA products. The shikimate pathway products phenylalanine and tyrosine are proposed to be processed to 4-hydroxydihydrocinnamaldehyde (4-HDCA, **4**) and dopamine (**3**), respectively, which are then joined through a Pictet–Spengler reaction to form the 1-phenethylisoquinoline (**1**) scaffold. Solid arrows indicate identified steps, and the dashed arrows show unknown modification reactions. (B) Heterologous pathway of **1** in tobacco for the production of colcine precursors. (C) Heterologous production of **1** in microbes from multicarbon precursor. L-DOPA (**2**), levodopa; 4-HPP, 3-(4-hydroxyphenyl) propanol; PAL, phenylalanine ammonia-lyase; C4H, cinnamate 4-hydroxylase; 4CL, 4-coumarate CoA ligase; CCR, cinnamoyl-CoA reductase; DBR, NADPH-dependent double-bond reductase; AER, NADPH-dependent 2-alkenal reductase; TYR, tyrosinase; TyrH, tyrosine hydroxylase; DODC, tyrosine/DOPA decarboxylase; PSS, 1-phenylethylisoquinoline scaffold synthase; OMT, O-methyltransferase; NMT, N-methyltransferase; CYP, cytochrome P450; CAR, carboxylic acid reductase; NOX, NAD(P)H oxidase; ADH7, alcohol dehydrogenase 7.

recently designed an artificial enzymatic cascade starting from 3-(4-hydroxyphenyl) propanol (4-HPP), which was dehydrogenated to the corresponding aldehyde **4** by the yeast-derived alcohol dehydrogenase ADH7 with the aid of *Streptomyces*-derived NAD(P)H oxidase (NOX) variant [21] (Fig. 1C). Then **3** and **4** were condensed to **1** by CjNCS, forming a three-enzyme cell-free system that finally produced 5.4 mM of **1**. In addition to the alcohol (4-HPP)-starting pathway, an alternative four-enzyme biocatalytic cascade has been recently developed by Gao et al. to biosynthesize (*S*)-autumnaline and its various derivatives in *E. coli* (yields of 1.9–3.9 mM) [22] (Fig. 1C). In this system, a carboxylic acid reductase (CAR) from *Tsukamurella paurometabola* was introduced to convert phenylpropanoic acids to phenylpropionic aldehydes (structural analogues of **4**), and the PIAs backbone was constructed from phenylpropionic aldehydes and **3** by NCS from *Thalictrum flavum*. However, these artificial pathways required the addition of multicarbon precursor in vitro, which may increase the production costs.

In this study, we successfully established a heterologous biosynthetic pathway for the de novo synthesis of 1-phenethylisoquinoline (**1**) in the prokaryotic *E. coli* from simple carbon source. The yield of the key intermediate 4-HDCA (**4**) was optimized by screening different AERs, enhancing NADPH supply, and site-directed mutagenesis of the key enzyme ChAER1. An endogenous reductase-deficient *E. coli* strain with high tyrosine production and modified dopamine (**3**) pathway was constructed, allowing an efficient de novo synthesis of **1** (402.58 mg/L in a 5L fermenter), which lays the foundation for the scalable production of value-added PIAs in the future.

2. Materials and methods

2.1. Materials and chemicals

The leaf needles of *C. harringtonia* and the rhizomes of *G. superba* were collected and used in this work. *E. coli* strains DH10B and BL21 (DE3) were grown in Luria-Bertani (LB) broth. The 1-phenethylquinoline (**1**) authentic sample was purchased from Wuhan Anjiekai Biomedical Science and Technology Co., Ltd, (Wuhan, China). *p*-Coumaric acid and *p*- Coumaraldehyde was purchased from Yuanye Biotechnology Co., Ltd., (Shanghai, China). L-Tyrosine was purchased from Sangon Biotech (Shanghai, China). L-DOPA, tyramine and dopamine were purchased from Sigma-Aldrich (Merck, Germany).

2.2. RNA isolation and plasmid constructions

Total RNA of *C. harringtonia* and *G. superba* were extracted using AxyPrep Multisource Total RNA Miniprep Kit (Axygen Biosciences, CA, U.S.A). RNA purity was checked by Agilent 2100 Bioanalyzer (Agilent, CA, U.S.). The total RNA was subsequently digested by DNaseI (Takara, Japan) for 30 min. The cDNA of *C. harringtonia* and *G. superba* was synthesized using PrimeScript RT reagent Kit with gDNA eraser (Takara, Japan). The fragments of *ChAER1*, *ChAER2* and *GsAER* were amplified from the cDNA by PCR using high-fidelity PrimeSTAR Max DNA polymerase (Takara, Japan) and gene-specific primers (Supporting Information, Table S2). The PCR products were purified, double-digested with *Nde*I/*Not*I (NEB, U.S.A.) and subsequently ligated into pre-digested pET-28a to give pMYP208-210, respectively. The *E. coli* codon-optimized *GsAER* was subcloned and inserted into the *Nde*I/*Not*I sites of pET-28a to give pMYP211.

The open reading frames of *RsTAL*, *Pc4CL* and *AtCCR1* were amplified from cloning vectors and subcloned into the vector pET-28a between *Xba*I/*Eco*RI (for *Pc4CL*) [23]. *Eco*RI/*Sac*I (for *RsTAL*) and *Sac*I/*BamH*I (for *AtCCR1*) via ClonExpressII One Step Cloning Kit (Vazyme Biotech, Nanjing, China), resulting in pMYP203. Subsequently, the *AER* fragments were PCR-amplified and ligated into *BamH*I and *Avr*II digested pMYP203 to give pMYP204-207, respectively.

For pMYP225 (pACYC-T7-*muTyrH-RnPCD-RnQDHPR-PpDODC-Δ24-CjNCS*-T7ter) construction, the *PpDODC* fragment was PCR-amplified and ligated into *Not*I and *Xho*I digested pQZ79 [24], generating pMYP224 (pACYC-T7-*muTyrH-RnPCD-RnQDHPR-PpDODC*-T7ter). The codon-optimized and 24 amino acids-truncated (Δ24)-CjNCS was subcloned and inserted into *Spe*I/*Not*I of pMYP224 to give pMYP225. The *PpDODC-Δ24-CjNCS* fragment was PCR-amplified and ligated into *Xba*I and *Spe*I sites digested pET-28a, generating pMYP226. Subsequently, the codon-optimized *HpaBC-D11* was subcloned and inserted between the *PpDODC* and *Δ24-CjNCS* fragments via one-step cloning to give pMYP227. All plasmids and strains used in this study are provided in Table S5.

2.3. Media and cultivations

E. coli was cultured in LB medium (10 g/L tryptone, 5 g/L yeast extract, 10 g/L NaCl) for gene cloning, plasmid propagation, and preparation of culture seeds. M9Y medium containing 1 × M9 minimal salts, 2 % glucose, 0.05 % yeast extract, 0.1 mM $CaCl_2$, and 2 mM $MgSO_4$ was used for tyrosine-feeding shake flask cultivation of recombinant *E. coli* strains. Before cultivation, M9Y medium was supplemented with 1000 × trace metal mix (0.03 g/L H_3BO_3, 1 g/L thiamine, 0.5 g/L $CoCl_2$, 0.94 g/L $ZnCl_2$, 1.6 g/L $MnCl_2$, 3.6 g/L $FeCl_2$, 0.38 g/L $CuCl_2$). Kanamycin (50 mg/L), chloramphenicol (34 mg/L), and spectinomycin (50 mg/L) were added to the medium as needed. Recombinant *E. coli* strains for de novo tyrosine production were fermented in shake flask using TB2 medium with the following formulations: 2 % tryptone, 2.4 % yeast extract, 72 mM K_2HPO_4, 17 mM KH_2PO_4, 0.4 % glycerol, 2 % glucose was added before cultivation. Kanamycin (50 mg/L), carbenicillin (100 mg/L), and spectinomycin (50 mg/L) were added to the medium as needed.

For abovementioned shake flask fermentation, single clones of *E. coli* strains were inoculated into 2 mL of liquid LB medium and grown at 37 °C overnight with shaking at 250 rpm. Then 400 μL of the pre-inoculums were add to a 100 mL flask containing 20 mL of M9Y or TB2 medium at 37 °C with shaking at 250 rpm, until OD_{600} reached 0.5. Isopropyl-β-D-thiogalactoside (IPTG) was added to a final concentration of 0.1 mM and L-tyrosine was added to a final concentration of 500 mg/L. The cultures were then incubated at 22 °C and 220 rpm for production of the target compounds. After 72 h fermentation, samples were collected for analyses. Samples used for HPLC−MS analyses were sonic disrupted, then extracted three times with an equal volume of butyl alcohol. The supernatant was evaporated to dryness and dissolved in 200 μL of acetonitrile; 20 μL was injected for HPLC−MS analysis. The samples for HPLC analysis were subjected to ultrasonic fragmentation of cells, and 1 M HCl in equal volume was added and incubated at 37 °C for 30 min, then centrifuged at 12000 rpm for 10 min, and 20 μL of supernatant was subjected to HPLC analysis.

2.4. Fed-batch fermentation

Fed-batch fermentation was carried out using a 5 L of bioreactor containing 1 L of total working volume at 22 °C and pH 7.0. The fed-batch fermentation broth contained 20 g/L glucose, 12 g/L K_2HPO_4, 4.2 g/L KH_2PO_4, 2 g/L $(NH_4)_2SO_4$, 1.2 g/L $MgSO_4{\cdot}7H_2O$, 1.7 g/L citric acid, 0.5 g/L yeast extract and 1 × trace metal mix. The feeding solution contained 600 g/L glucose, 10.7 g/L $(NH_4)_2SO_4$ and 1 × trace metal mix. Seed culture was prepared by inoculating single clones into a 2 mL LB liquid medium and grown at 37 °C for 12 h, then 1 mL of the pre-inoculum was added to a 250 mL flask containing 50 mL of LB liquid medium at 37 °C with shaking at 250 rpm for 6 h. The seeds were transferred into the bioreactor, making a 5 % (v/v) inoculum size. Fermentation was performed at 37 °C with an air flow rate of 1 vvm. The pH was controlled at 7.0 by the ammonia solution (25 %, v/v). When OD_{600} reached 10−15, 0.5 mM IPTG, 2 g/L sodium malonate dibasic, and 500 mg/L L-phenylalanine or 500 mg/L L-tryptophan were added into the broth, and the temperature was adjusted to 22 °C. Samples were obtained for cell growth assay and HPLC analyses.

2.5. CRISPR-Cas9 mediated genome editing

The CRISPR-Cas9 system containing two plasmids, pCas9 and pTargetF, was used for consecutive gene knockouts and integration. N20 sequences paired with the target of interest were designed online at https://benchling.com. For chorismite overproduction, aroC was integrated into the *lacZ* locus of the sQZ19 genome [24]. The Trc promoter is upstream of aroC and the T7 terminator is downstream. For trpE, dkgB, yqhC, yqhD, yahK, yeaE, dkgA, and yjgB knockout, we constructed the plasmid containing appropriate regions for knockout before the preparation of the PCR fragment. PCR-based method was adopted for genome editing. For details, see reference [25]. The pCas9 and pTarget were introduced into *E. coli* cells by electrotransformation. Correct transformants of strain sMYP7k, sMYP8k and sMYP9k were identified by PCR and DNA sequencing methods. All primers and N20 sequences were listed in Table S3.

2.6. Protein expression of ChAER1, ChAER2, GsAER and GsAERopt

The expression vectors of ChAER1, ChAER2, GsAER, and GsAERopt were transformed into BL21(DE3) for expressing recombinant AER proteins. The empty vector pET-28a transformed into BL21(DE3) was used as the blank control. A positive colony was picked from the plate and inoculated into a 100 ml flask containing 10 mL LB culture with kanamycin (50 μg/mL) and grown at 37 °C, 200 rpm for 12 h. The overnight seed culture was inoculated (1:100) to 500 mL flask containing 100 mL LB. Induction was performed with 0.1 mM IPTG at OD_{600} of 0.4–0.6, and further cultivated at 16 °C, 22 °C or 28 °C and at 200 rpm for 20 h. The fermentation cultures were centrifuged to separate the supernatant and the cells. The cells were suspended by buffer A (20 mM Tris-HCl, pH 8.0, 100 mM NaCl), mixed with 1 mM phenylmethylsulfonyl fluorid (PMSF, Sigma, Germany), 2 mM $MgCl_2$ and 5 μg/mL DNaseI, and placed on ice for 30 min. The cells were crushed under high pressure and centrifuged at 12000 g at 4 °C for 90 min. For all *E. coli* strains, the soluble expression of ChAER1, ChAER2, GsAER, and GsAERopt were examined by SDS-PAGE analysis.

2.7. Protein structure prediction, molecular docking and site-directed mutagenesis

The protein structure of ChAER1 was predicted by Robetta (https://robetta.bakerlab.org/), the protein model was established using raspberry ketone synthase (PDB ID:6EOW) as the template [26]. AutoDockTools (v1.5.6) was used for the preparing the protein models and the substrates NADPH and 4-HDCA. Molecular docking of ChAER1 and substrates was performed with AutoDock_Vina [27]. A grid box of 30 × 30 × 30 potentially encompassed the substrate binding was set as the search space. The generated models with docked 4-HDCA in appropriate position were then used for design of mutants. Site-directed mutagenesis of candidates was carried out using a Fast Mutagenesis System (TransGen Biotech Co., Ltd., China). Briefly, the mutations were introduced into pMYP206 by specific primers listed in Table S4, giving pMYP212~223. The resulted mutants pMYP212~223 were further subcloned into the *Bam*HI and *Avr*II sites of pMYP203 via ClonExpress II One Step Cloning Kit. For the functional characterization of these mutants, pMYP212~223 were individually transferred with pZY11 and pMYP225 into *E. coli* BL21(DE3) (strains sMYP221-233). The cultivation and extraction of *E. coli* strains were identical to that of sMYP203.

2.8. In vitro enzymatic assay and kinetic studies of AERs

A typical enzymatic assay was performed in a 500 μL aliquot of reaction mixture containing 50 mM Tris-HCl (pH 7.5), 1 mM NADPH, 10 μM–2.5 mM *p*-coumaraldehyde, and 50 μL crude enzymes. The reaction mixtures were incubated at 30 °C for 1 h and finally quenched by 500 μL ethyl acetate and vortexed vigorously. The quenched reaction mixtures were extracted three times with 500 μL ethyl acetate, and the combined organic layers were evaporated to dryness. The enzyme kinetic parameters were calculated by quantification of the formation of **4**. Michaelis–Menten curves were generated by GraphPad Prism 8.

2.9. HPLC and HR-MS analysis

For the detection of **1**, the diluted fermentation mixtures were subjected to HPLC analyses (Dionex UltiMate 3000 SD HPLC system, Thermo Scientific, MA, U.S.A.). The separation was achieved on a C18 column [SilGreen ODS column (φ4.6 × 250 mm, S-5 μM), Greenherbs Co., Ltd., Beijing, China] with a flowrate of 1.0 mL/min at 30 °C. A linear gradient elution was performed with mobile phases containing acetonitrile with 0.1 % trifluoroacetic acid (A) and H_2O with 0.1 % trifluoroacetic acid (B): 0.0–10.0 min, 5%–95 % A in B; 10.0–12.5 min, maintaining 95 % A; 12.5–15.0 min, re-equilibrating to the initial condition. The UV absorption was monitored at λ = 280 and 254 nm. Ultra-performance liquid chromatography-high resolution-tandem mass (UPLC-HR-MS/MS) spectra were acquired using Q Exactive hybrid quadrupole-Orbitrap mass spectrometer (Thermo Scientific, U.S.A.) equipped with an Acquity UPLC BEH C18 column (φ2.1 × 50 mm, 1.7 μM, Waters, U.S.A.). A linear gradient was set with mobile phases containing acetonitrile (A) and H_2O with 0.1 % formic acid (B) as follows: 20 %–100 % (16 min) A in B, 100 % A maintained for 5 min. The flow rate was 0.5 mL/min. The mass acquisition was performed in negative ionization mode with full scan (50–1000). For the detection of **4** in enzymatic assays, the methanol-redissolved reaction mixtures were subjected to HPLC equipped with a C18 column [SilGreen ODS column (φ4.6 × 250 mm, S-5 μM), Greenherbs Co., Ltd., Beijing, China]. The flowrate was 0.5 mL/min and the column oven temperature was 30 °C. A linear gradient elution was performed with mobile phases containing methanol (A) and H_2O with 0.1 % formic acid (B): 0–5 min, 5%–55 % A in B; 5–14 min, 55%–90 % A in B; 14–18 min, re-equilibrating to 5 % A in B; 18–25 min, maintaining 5 % A. The UV absorption was monitored at λ = 280 nm.

3. Results and discussion

3.1. Design and establishment of artificial pathway to phenylethylisoquinoline

According to the elucidated pathway, the biosynthesis of **1** scaffold recruits two precursors **3** (from L-tyrosine) and **4** (from L-phenylalanine) (Figs. 1 and 2A). To this end, we initially divided the whole pathway into two modules, defining them as Module 1 (synthesizing **3**, Fig. 2A, blue arrow) and Module 2 (synthesizing **4**, Fig. 2A, red arrow). Module 1 includes MuTyrH (from mouse) and PpDODC (from *Pseudomonas putida* KT2440) essential for the production of **3**, as well as the genes for reinforcement of tetrahydromonapterin (MH_4) supply. The *E. coli* host naturally produced MH_4 cofactor which serves as the microbial counterpart of tetrahydropterin (BH_4) that is required for TyrH activity. These pterin cofactors could be regenerated from 4α-hydroxytetrahydrobiopterin by two enzymes, pterin-4α-carbinolamine dehydratase (RnPCD) and dihydropteridine reductase (RnQDHPR) (Fig. 2A) [28–30]. Module 2 encompasses genes encoding enzymes responsible for *p*-coumarate biosynthesis and two downstream reductases, namely CCR from *Arabidopsis thaliana* (AtCCR1) and AER from *Gloriosa superba* (GsAER) [19,31]. In higher plants, the *p*-coumarate pathway is largely shared by lignin, flavonoid and cumarin biosynthesis, which may involve a triple gene set (PAL-C4H-4CL) starting from L-phenylalanine or a dual gene set (TAL-4CL) starting from L-tyrosine [23,32,33]. To simplify the pathway, we replaced the natural pathway catalyzing phenylalanine to **4** (Fig. 2A, gray arrow) with a tyrosine-starting one, bypassing the handling of cytochrome P450 (CYP) enzyme C4H. Finally, the Module 1-produced **3** and Module 2-produced **4** is expected to be joined by Pictet–Spengler condensation to give the **1** scaffold. In *Cephalotaxus hainanensis*, this step

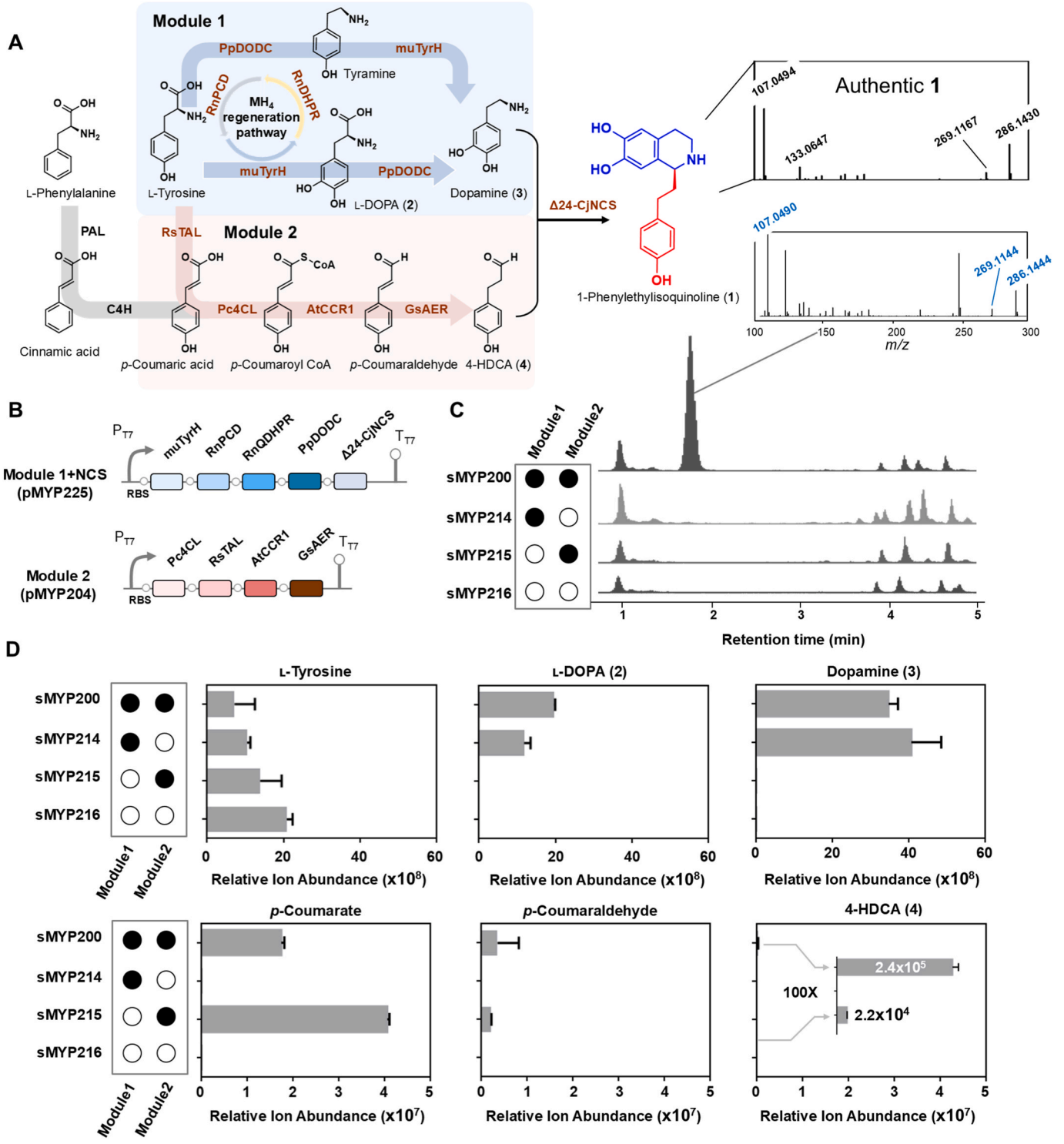

Fig. 2. Artificial biosynthetic pathway construction. (A) Schematic diagram of synthesis of **1** from L-tyrosine and L-phenylalanine. The blue arrows correspond to module 1 and the red arrows correspond to module 2. (B) Construction of plasmids for production of **3** and **4**. (C) High performance liquid chromatography (HPLC)-high resolution mass (HRMS) analysis of *E. coli* extracts co-expressed with two modules (500 mg/L tyrosine was exogenously added as substrate). (D) Pathway products accumulated in different strains harboring module 1 and module 2. RsTAL, tyrosine ammonia-lyase from *Rhodobacter sphaeroides*; Pc4CL, 4-coumarate CoA ligase from *Petroselinum crispum*; AtCCR1, cinnamoyl-CoA reductase from *Arabidopsis thaliana*; GsAER, NADPH-dependent alkenal reductase from *Gloriosa superba*; muTyrH, tyrosine hydroxylase from mouse; PpDODC, tyrosine/DOPA decarboxylase from *Pseudomonas putida*; RnQDHPR, dihydropteridine reductase from *Rattus norvegicus*; RnPCD, pterin-4α-carbinolamine dehydratase from *Rattus norvegicus*; Δ24-CjNCS, 24 amino acid truncated (*S*)-norcoclurine synthase from *Coptis japonica*.

is accomplished by ChPSS, which promiscuously fuses **4** or 4-hydroxyphenylacetaldehyde (4-HPAA) with **3**, forming **1** or (*S*)-norcoclaurine respectively [9]. Considering the structural similarity of **4** and 4-HPAA, it is likely that such plant Pictet–Spenglerases generally recognize both substrates, as is also observed in the (*S*)-norcoclurine synthases (NCSs)-mediated BIAs biosynthesis in *Coptis* species and lotus [34]. We here attempt to use a well-tested NCS enzyme, CjNCS1 from *Coptis japonica*, as an alternative of ChPSS. The N terminus-truncated

Δ24-CjNCS1 has been proved working functionally in *E. coli* and tobacco chassis, catalyzing the condensation reaction between **3** and various alkyl and aromatic aldehydes with considerable efficiency [16,19,35,36].

To achieve heterologous biosynthesis of **1** in *E. coli*, we therefore assembled plasmid pMYP225 harboring the Module 1 genes ligated with Δ24-*CjNCS1* and pMYP204 harboring the Module 2 genes (Fig. 2B). The constructed plasmids were co-expressed in *E. coli* BL21(DE3) supplemented with 500 mg/L L-tyrosine, and the culture extracts were detected by UPLC-Q-TOF-MS/MS analysis. After 5 days fermentation, as shown in the LC-MS charts, the strain co-expressing both modules (sMYP200) produced one peak with $[M+H]^+$ ion peak appeared at $m/z = 286.1444$, which was identical to that of the authentic sample of **1** (Fig. 2A and C). In the strains expressing module 1 and module 2 alone, only the module-specific product **3** and **4** were detected, respectively, with the absence of the final product **1**. To the best of our knowledge, this is the first attempt of de novo synthesis of **1** from simple carbon source.

In strain sMYP200 co-expressing module 1 and 2, we noticed that the major accumulated intermediate in module 2 was *p*-coumaric acid, while the yields of downstream reduced product *p*-coumaraldehyde and **4** dropped significantly by orders of magnitude (Fig. 2D), which clearly indicated that the following reductases CCR and AER should be optimized. Moreover, we also detected in module 1 redundant tyrosine and abundant accumulation of various intermediates that were much higher than module 2 products (Fig. 2D), which also prompted us to make necessary optimization of the flux of this module. Such metabolic profiles are consistent with those observed in the **1** biosynthesis using *N. benthamiana* [19]. In Nett and co-workers' research, individual expression of the **3** and **4** pathways resulted in the production of 2.3 ± 0.3 mg/g of **3** and 2.4 ± 0.8 μg/g of **4** in the tobacco chassis,

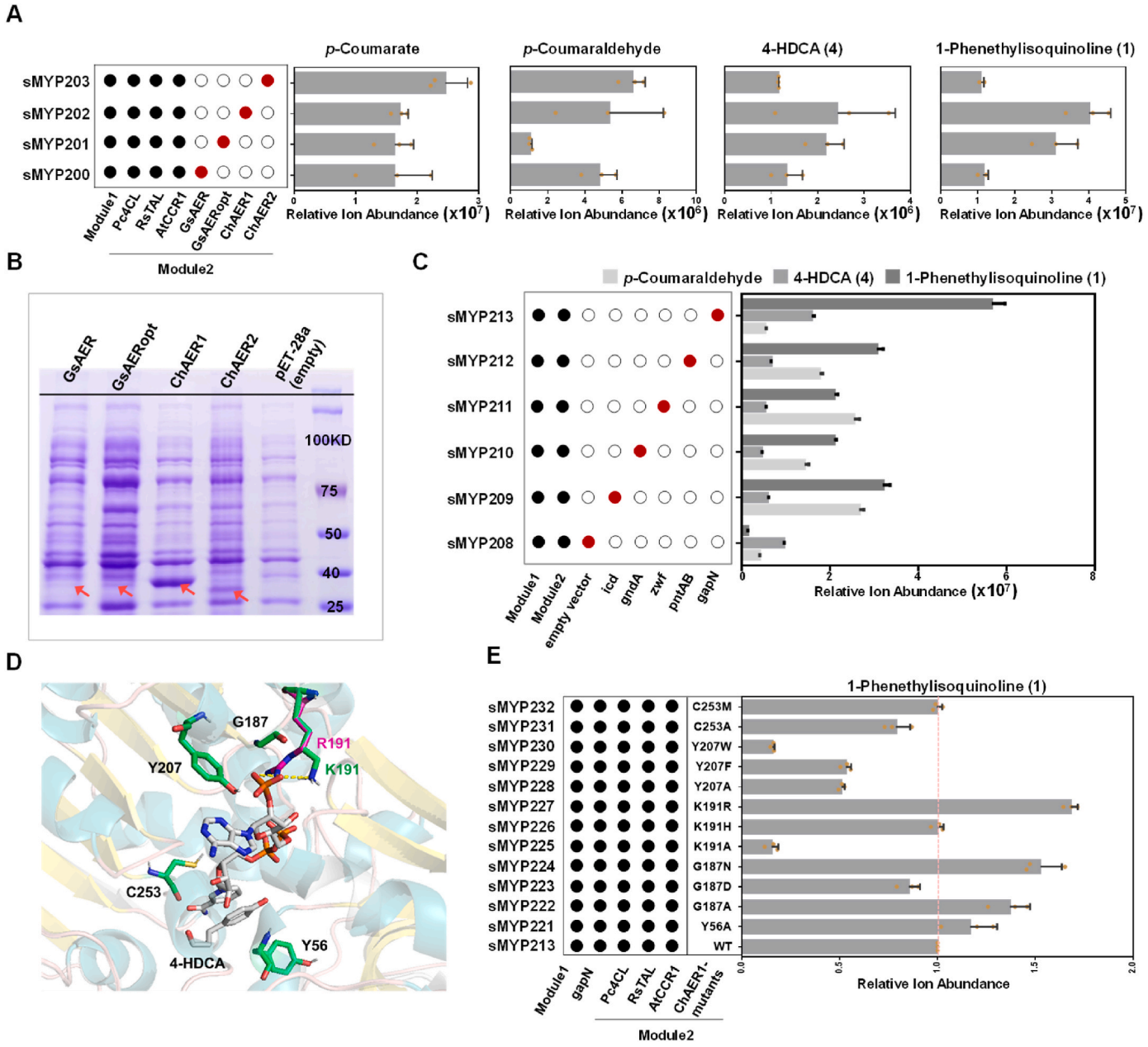

Fig. 3. Optimization of 2-alkenal reductases. (A) Production profiles of strains co-expressed with four 2-alkenal reductases from different species and Module 1 in *E. coli* with supplement of 500 mg/L tyrosine. (B) Protein expression of different AERs in *E. coli*. (C) Production profiles of strains co-expressed with NADPH-regenerating enzymes. (D) The Robetta-predicting 3D structure of ChAER1 was docked with NADPH and *p*-coumaraldehyde, revealing key residues in the substrate binding pocket. (E) Relative yields of **1** by ChAER1 mutants (the yield of **1** by wild-type ChAER1 was normalized to 100 %).

respectively, which clearly indicated an imbalance between the metabolic flux to **3** from L-tyrosine and that to **4** from L-phenylalanine. On the other hand, Zhang and Gao et al. used a cell-free system [21] and a whole-cell catalysis [22] for the heterologous synthesis of **1**, respectively, in which the addition of substrates can be adjusted to the appropriate stoichiometric ratio, avoiding the problem of in vivo flow imbalance that may be caused by the de novo synthesis.

Similar to the biosynthesis of PIA, the synthesis of BIAs also requires two precursors, **3** and 3,4-dihydroxyphenylacetaldehyde (3,4-DHPAA) (Fig. S1). 3,4-DHPAA can be formed from **3** by monoamine oxidase (MAO) [13,24], therefore the bottleneck of the imbalance between these two substrates lies in the low activity of MAO, rather than the *p*-coumarate pathway involved as in PIA biosynthesis. We speculated that the problem caused by AER-mediated reduction is specific to PIA biosynthesis, but is universal in different chassis cells, which needs to be solved in subsequent experiments.

3.2. Optimization of NADPH-dependent 2-alkenal reductase

The abovementioned metabolic profile of strain sMYP200 suggested an urgent need of optimizing the NADPH-dependent alkenal reductases (AERs) in module 2. We first carried out screening of the AERs from different species. In the transcriptome assembly of *Cephalotaxus harringtonia*, there are two AER-encoding genes, namely ChAER1 and ChAER2. In addition to the ChAERs, the AER from *Gloriosa superba* (GsAER) was codon optimized to facilitate better performance in the *E. coli* host. Different AERs were introduced to the Module 2 plasmids and co-expressed with the Module 1 plasmid (Fig. 3A). According to the quantitative LC-MS analysis, the strain carrying ChAER1 (strain sMYP202) had the highest production of **1**, which was about 3.48 times that of GsAER (Fig. 3A). In the codon-optimized GsAER (GsAERopt) strain, the yield of **1** also increased to about 1.52 times that of the wild type. The SDS-PAGE further supported the better performance of ChAER1, because that the soluble expression of ChAER1 was significantly higher than that of other AERs (Fig. 3B), which was even better than GsAERopt. Although enzyme kinetics analysis indicated that the K_m value of GsAER (319.3 μM) was lower than that of ChAER1 (466.8 μM), which suggested GsAERopt had higher affinity for *p*-coumaraldehyde (Fig. S2), we speculated that the better soluble expression of ChAER1 made up for the lack of affinity, giving ChAER1 a performance better than GsAER. Further solubility optimization suggested that lower IPTG induction at 28 or 22 °C may be more conducive to the expression of ChAER1 (Fig. S3).

Since the activity of reductases require the cofactor NADPH, we next incorporated several canonical NADPH-generating enzymes, including gapN (NADP-dependent glyceraldehyde-3-phosphate dehydrogenases) from *Clostridium* sp., and endogenous pntAB (pyridine nucleotide transhydrogenase), zwf (NADP-dependent glucose-6-phosphate dehydrogenase), icd (isocitrate dehydrogenase) and gnd (6-phosphogluconate dehydrogenase) to enhance the supply of NADPH [37]. Co-expression of these dehydrogenases with the module 1 and module 2 resulted in strains sMYP208-213 (sMYP208 harboring empty vector was used as control) (Fig. 3C). The intermediates and the final product **1** were detected by LC-MS, which showed that the titer of module 2 product **4** and the final product **1** increased significantly in the strains sMYP209-213 with enhanced cofactor supply. The strain sMYP213 overexpressing gapN showed the highest yield of **1** with less accumulation of *p*-coumaraldehyde.

To further increase the conversion of *p*-coumaraldehyde to **4**, we then carried out site-directed mutagenesis to improve the enzymatic activity of ChAER1. Although there are currently no reports on the protein structure of ChAERs and ChDBRs, we selected a three-dimensional crystal structure of a NADPH-dependent DBR, namely raspberry ketone synthase (RKS, PDB ID: 6EOW) as a template to model ChAER1. The RKS protein shares 72 % sequence similarity with ChAER1 and was found to be able to convert 4-hydroxybenzalacetone (a structural analogue of **4**) into raspberry ketone [26]. In the constructed ChAER1 structure, we noticed the π-π stacking between the ligand **4** and the nicotinamide aromatic rings of NADPH, which sandwiched with residues Y56 and C253 (Fig. 3D). A hydride transfer distance of 3.3 Å from NADPH to the alkene double bond of **4** was estimated. As observed in the related structures [20,26,38]. the binding pockets also involves several key residues, which correspond to G187, K191 and Y207 in ChAER1. We proposed that NADPH cofactor could specifically bound in a triad of hydrogen bond-based contacts with the G187 backbone nitrogen and the side chains of K191 and Y207, and K191 was considered to interact with either the ribose 5′-phosphate (within 3.9 Å distance) or the neighboring 4′-hydroxyl group (3.4 Å). Accordingly, we generated a series of ChAER1 mutants including Y56, G187 (corresponding to G191 in RKS), K191 (K195 in RKS), Y207 (Y211 in RKS) and C253. We found that the yield of **4** increased by 1.69 times when K191 was mutated to R. In $ChAER_{K191R}$ mutant, the spatial distance between arginine and the ribose 5′-phosphate group of the cofactor diminished from 3.9 Å to 1.5 Å, which was thought to be responsible for the increasing yield. While in the case of altering K191 into alanine, the production of **1** was significantly reduced. This result is also supported by the previous structure-guided engineering of RKS, in which K195 (corresponding to K191 in ChAER1) was found to be a key residue interacting with the 4′-hydroxyl group of both NADPH and NADH [26].

In addition to the *in planta* biosynthesis of **4** by AER-catalyzed α,β double bond reduction, the utilization of phenylpropionic alcohol or acid as starting materials to construct the artificial **4** synthesis has also been reported [21,22]. In such cases, while both ADH7 and CAR could generate **4** or its analogue, their activity toward the non-natural substrates was relatively low due to broad substrate spectrum. The modification of ADH7 was not successful as the catalytic activity of ADH7 variants was comparable to that of wild-type ADH7 without obvious increase. In our research, the well expressed ChAER1 was used for the biosynthesis of **4**, and its variants K191R, G187 N and Y56A showed enhanced **1**-producing ability. Overall, the yield of **1** was optimized from 35.73 mg/L to 60.53 mg/L in shake-flask fermentations through screening AER genes with better expression, enhancing cofactor supply and key enzyme engineering that promoted the enzymatic activity catalyzing the formation of **4**.

3.3. Optimization of de novo dopamine production

After optimization of the Module 2 enzymes, we then set out to increase the production of **3** in Module 1 and the final product **1** by engineering of the *E. coli* host. We first aim to construct a L-tyrosine-overproducing strain in line with several successful strategies used for high-yield production of shikimate pathway products (Fig. 4A). This involves overexpression of a set of key enzymes in the biosynthesis of L-tyrosine [39]. which includes ppsA (phosphoenolpyruvate synthase), tktA (transketolase I), aroE (dehydroshikimate reductase), aroC (chorismate synthase) [40]. and two feedback-resistant mutants $tyrA^{fbr}$ and $aroG^{fbr}$. The regulatory suppressor-encoding *TyrR* was inactivated by CRISPR-Cas9 to alleviate the feedback inhibition, while *pheA* in L-phenylalanine pathway and *trpE* in L-tryptophan pathway were knocked out to eliminate the competence with tyrosine precursors [41]. On the other hand, since one of the major barrier to overproduce aromatic aldehydes in engineered *E. coli* is that multiple endogenous enzymes quickly convert desired aldehydes into unwanted alcohols [42]. we further deleted six ADH genes encoding aldo-keto reductases (*dkgB*, *yeaE* and *dkgA*), alcohol dehydrogenases (*yqhD*, *yahK* and *yjgB*) and a transcription factor *yqhC* in the *E. coli* host to avoid reduction of the targeted aldehydes (Fig. 4A). Such strategy was recently adopted by Gao et al. in the biosynthesis of (*S*)-autumnaline [22]. The resulted strain sMYP9k was able to produce 1183.5 mg/L tyrosine from glucose (Fig. 4B), which was much higher than the level of tyrosine previously supplemented.

Subsequently, we replaced TyrH and the related MH_4 recycle system

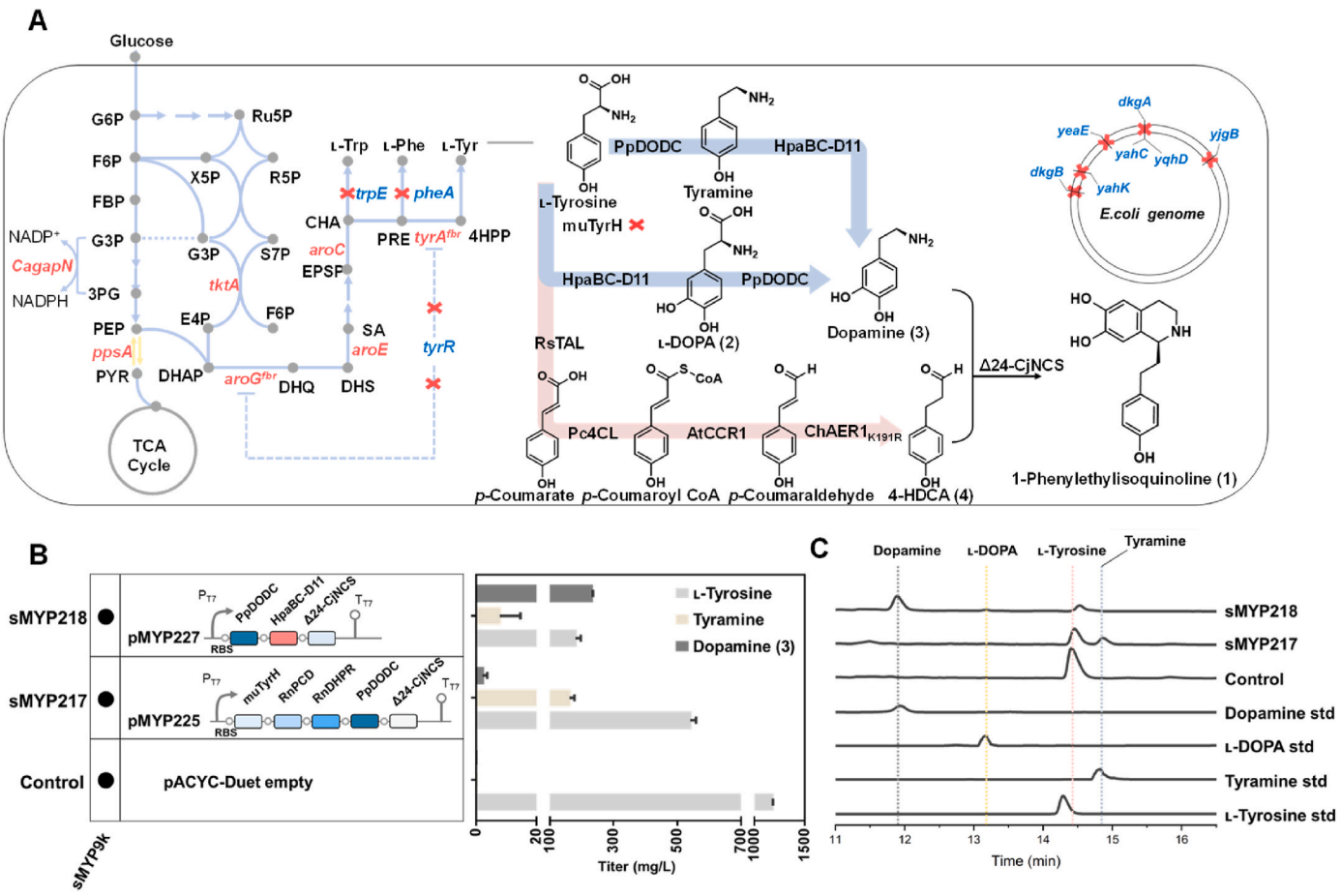

Fig. 4. Optimization of dopamine synthesis. (A) Schematic diagram of synthesis of **1** from glucose in engineered *E. coli* strain sMYP9k. Genes disrupted are shown in blue, and the overexpressed genes are marked in red. (B) Plasmid of new synthetic Module1 for production of **3** through introducing HpaBC-D11 and products accumulated in the engineered *E. coli* strains sMYP9k (control), sMYP217 and sMYP218. (C) HPLC analyses of tyrosine-related intermediates in module 1 produced by engineered *E. coli* strains sMYP9k (control), sMYP217 and sMYP218. Std, the abbreviation of standard. tktA, transketolase I; ppsA, phosphoenolpyruvate synthase; aroG, 3-deoxy-*d*-arabino-heptulosonate-7-phosphate synthase; aroE, dehydroshikimate reductase; aroC, chorismate synthase; pheA, chorismite mutase/prephenate dehydratase; tyrA, chorismate mutase/prephenate dehydrogenase; trpE, anthranilate synthase; CagapN, glyceraldehyde-3-phosphate dehydrogenase from *Clostridium acetobutylicum*; PEP, phosphoenolpyruvate; PYR, pyruvate; G6P, glucose-6-phosphate; F6P, fructose-6-phosphate; FBP, fructose-1,6-biphosphate; G3P, glyceraldehde-3-phosphate; 3 PG, 3-phosphoglycerate; Ru5P, ribulose-5-phosphate; R5P, ribose-5-phosphate; X5P, xylulose-5-phosphate; S7P, sedoheptulose-7-phosphate; E4P, D-erythrose 4-phosphate; DAHP, 3-deoxy-*d*-arabino-heptulosonate-7-phosphate; DHQ, 3-dehydroquinate; DHS, 3-dehydroshikimate; SA, shikimate; S3P, shikimate-3-phosphate; EPSP, 5-enolpyruvylshikimate 3-phosphate; CHA, chorismate; PRE, prephenate; 4HPP, 4-hydroxyphenylpyruvate; TCA cycle, tricarboxylic acid cycle; L-tyr, L-tyrosine; L-phe, L-phenylalanine; L-Trp, L-tryptophan.

with a single gene encoding a mutant of HpaBC (HpaBC-D11, from *E. coli*). It has been reported that the two-component flavin-dependent monooxygenase HpaBC can hydroxylate multiple phenol compounds [43–45], while its mutant D11 particularly favors the conversion of tyramine to **3** [46]. Hence HpaBC-D11 was introduced to a new Module 1 plasmid pMYP227, and expressed in sMYP9k (strain sMYP218) to evaluate the production of **3** by shake-flask fermentation. The plasmid pMYP225 harboring TyrH-MH_4 recycle was also tested as control (strain sMYP217). Compared to the control strain sMYP217 (producing 179.3 mg/L tyramine and 3.4 mg/L **3** with 558.9 mg/L unconsumed tyrosine), strain sMYP218 yielded 234.2 mg/L of **3** from glucose, which was 68.9 times that of strain sMYP217. In addition, compared with sMYP217, the residual tyrosine (199.4 mg/L) and tyramine (3.3 mg/L) of sMYP218 were only 35.7 % and 1.84 % of those of sMYP217. Therefore, the newly introduced HpaBC efficiently guided the flux to the generation of **3** via tyramine, which not only alleviated the limitation caused by the TyrH-MH4-mediated tyrosine hydroxylation step, but also reduced the accumulation of tyramine as a by-product.

3.4. De novo biosynthesis and fed-batch fermentation of 1-phenylethylisoquinoline

The optimized Module 1 (pMYP227), Module 2 (pMYP218) and NADPH-enhancing gapN (pZY11) were co-expressed in the engineered *E. coli* sMYP9k, giving the strain sMYP220 which was used for de novo synthesis of **1** from glucose. Strain sMYP219 harboring pMYP227, pMYP206 (containing wild-type ChAER1) and pZY11 was used as a control. The strains were first evaluated for the production of **1** by shake-flask fermentation. While the strain sMYP219 harboring wild-type ChAER1 produced **1** from glucose with a titer of 46.77 mg/L (Fig. 5A), the K191R-mutant strain sMYP220 produced 62.3 mg/L of **1**, which was 149.1 % higher than that in the control. Next the strain sMYP220 was cultured in a 5 L fermenter to evaluate its **1** production capacity. To stabilize the culture environment, we maintain the pH of the fermentation solution at 7.0 through phosphate buffers. Since the knockout of *pheA* and *trpE* led to the disability of synthesizing tryptophan and phenylalanine in the engineered *E. coli*, L-tryptophan and L-phenylalanine were added to the feed solution to the final concentration of 500 mg/L to promote cell growth and increase cell density. The **1** titer of strain sMYP220 reached to 402.58 mg/L at 110 h (Fig. 5B), which

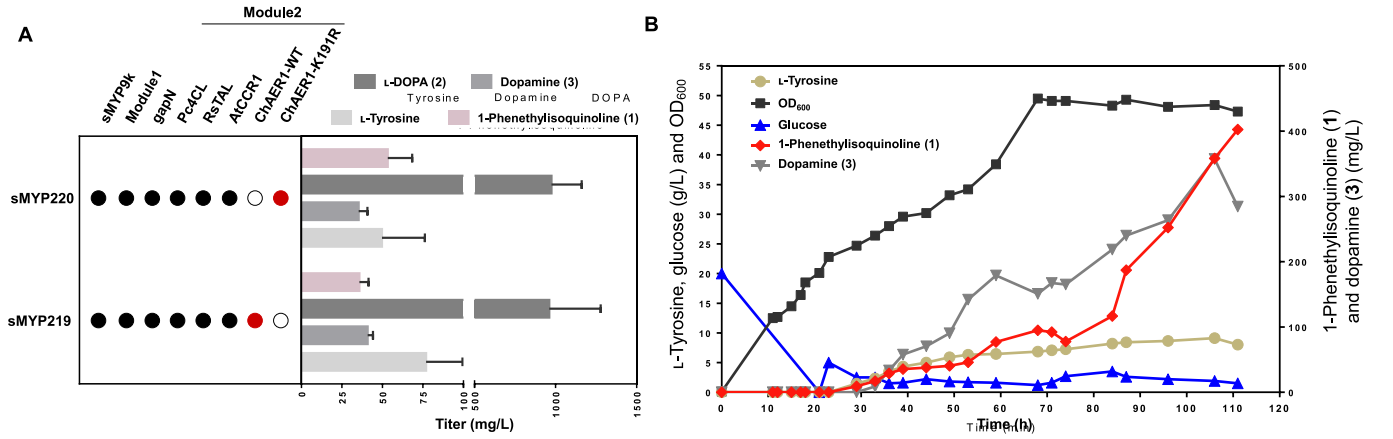

Fig. 5. De novo biosynthesis of 1-phenethylisoquinoline by strain sMYP219. (A) De novo biosynthesis of **1** in shake flask fermentation by strain sMYP219 and sMYP220. (B) De novo biosynthesis of **1** in a 5 L fermenter by strain sMYP220.

represented the highest titer of the de novo **1** biosynthesis to date.

CRediT authorship contribution statement

Yaping Mao: Writing – original draft, Visualization, Software, Methodology, Investigation, Formal analysis, Conceptualization. **Jiangming Zhu:** Writing – review & editing, Validation, Investigation. **Qian Zhang:** Methodology, Investigation. **Guangyi Wang:** Supervision. **Hongkai Fan:** Data curation, Investigation, Methodology. **Xiaowei Zhang:** Supervision. **Yuwei Sun:** Writing – review & editing, Writing – original draft, Visualization, Validation, Project administration, Formal analysis, Data curation, Conceptualization. **Yong Wang:** Writing – review & editing, Validation, Supervision, Project administration, Methodology, Investigation, Funding acquisition, Formal analysis, Data curation, Conceptualization.

Funding

This study was funded by the National Key R&D Program of China (2020YFA0907900, 2018YFA0900600, 2024YFA1700126), the National Natural Science Foundation of China (32070328), Derivative Bank of Chinese Biological Resources (KFJ-BRP-009-002), the Chinese Academy of Sciences Collaborative Innovation project (CNXT001), the Key Laboratory of Plant Carbon Capture, Chinese Academy of Sciences, the Key Laboratory of Plant Design, Chinese Academy of Sciences and the Foundation of Youth Innovation Promotion Association of the Chinese Academy of Sciences.

Declaration of competing interest

The authors declare no competing financial interest.

Acknowledgments

We thank Xiaoyan Xu in the Core Facility Centre of SIPPE for technical assistance with HPLC-HRMS acquisition. No conflict of interest is declared.

Appendix A. Supplementary data

Supplementary data to this article can be found online at https://doi.org/10.1016/j.synbio.2024.10.007.

References

[1] Plazas E, Avila MM, Muñoz DR, Cuca SL. Natural isoquinoline alkaloids: pharmacological features and multi-target potential for complex diseases. Pharmacol Res 2022;177:106126.
[2] Dey P, Kundu A, Kumar A, Gupta M, Lee BM, Bhakta T, et al. In: Sanches Silva A, Nabavi SF, Saeedi M, Nabavi SM, editors. Recent advances in natural products analysis. Elsevier; 2020. p. 505–67.
[3] Singh S, Pathak N, Fatima E, Negi AS. Plant isoquinoline alkaloids: advances in the chemistry and biology of berberine. Eur J Med Chem 2021;226:113839.
[4] Abdelkafi H, Nay B. Natural products from Cephalotaxus sp.: chemical diversity and synthetic aspects. Nat Prod Rep 2012;298:845–69.
[5] Lü S, Wang J. Homoharringtonine and omacetaxine for myeloid hematological malignancies. J Hematol Oncol 2014;7:2.
[6] Seca AML, Pinto D. Plant secondary metabolites as anticancer agents: successes in clinical trials and therapeutic application. Int J Mol Sci 2018;191.
[7] Slobodnick A, Shah B, Pillinger MH, Krasnokutsky S. Colchicine: old and new. Am J Med 2015;1285:461–70.
[8] Yang LPH. Oral colchicine (Colcrys): in the treatment and prophylaxis of gout. Drugs 2010;2710:1603–13.
[9] Qiao F, He Y, Zhang Y, Jiang X, Cong H, Wang Z, et al. Elucidation of the 1-phenethylisoquinoline pathway from an endemic conifer Cephalotaxus hainanensis. Proc Natl Acad Sci U S A 2023;1201:e2209339120.
[10] Ju X, Beaudry CM. Total synthesis of (-)-Cephalotaxine and (-)-Homoharringtonine via furan oxidation-transannular mannich cyclization. Angew Chem 2019;5820:6752–5.
[11] Eckelbarger JD, Wilmot JT, Epperson MT, Thakur CS, Shum D, Antczak C, et al. Synthesis of antiproliferative Cephalotaxus esters and their evaluation against several human hematopoietic and solid tumor cell lines: uncovering differential susceptibilities to multidrug resistance. Chemistry 2008;1414:4293–306.
[12] Marguerit M, Little G, Wang Y, He L, Allwein S, Reif J, et al. Total synthesis of [14C]-Labelled homoharringtonine. Eur J Org Chem 2015;201536:8003–10.
[13] Nakagawa A, Matsumura E, Koyanagi T, Katayama T, Kawano N, Yoshimatsu K, et al. Total biosynthesis of opiates by stepwise fermentation using engineered Escherichia coli. Nat Commun 2016;7:10390.
[14] Narcross L, Fossati E, Bourgeois L, Dueber JE, Martin VJJ. Microbial factories for the production of benzylisoquinoline alkaloids. Trends Biotechnol 2016;343:228–41.
[15] Zhao W, Liu M, Liu K, Liu H, Liu X, Liu J. An enzymatic strategy for the selective methylation of high-value-added tetrahydroprotoberberine alkaloids. Int J Mol Sci 2023;2420.
[16] Li Y, Li S, Thodey K, Trenchard I, Cravens A, Smolke CD. Complete biosynthesis of noscapine and halogenated alkaloids in yeast. Proc Natl Acad Sci U S A 2018;11517:E3922. e31.
[17] Galanie S, Thodey K, Trenchard IJ, Filsinger Interrante M, Smolke CD. Complete biosynthesis of opioids in yeast. Science 2015;3496252:1095–100.
[18] Trenchard IJ, Smolke CD. Engineering strategies for the fermentative production of plant alkaloids in yeast. Metab Eng 2015;30:96–104.
[19] Nett RS, Lau W, Sattely ES. Discovery and engineering of colchicine alkaloid biosynthesis. Nature 2020:5847819.
[20] Youn B, Kim SJ, Moinuddin SG, Lee C, Bedgar DL, Harper AR, et al. Mechanistic and structural studies of apoform, binary, and ternary complexes of the Arabidopsis alkenal double bond reductase At5g16970. J Biol Chem 2006;28152:40076–88.
[21] Zhang Y, Liu WQ, Li J. Constructing an artificial short route for cell-free biosynthesis of the phenethylisoquinoline scaffold. Synthetic and systems biotechnology 2023;84:610–7.

[22] Gao Y, Li F, Luo Z, Deng Z, Zhang Y, Yuan Z, et al. Modular assembly of an artificially concise biocatalytic cascade for the manufacture of phenethylisoquinoline alkaloids. Nat Commun 2024;151:30.
[23] Ji D, Li J, Xu F, Ren Y, Wang Y. Improve the biosynthesis of baicalein and scutellarein via manufacturing self-assembly enzyme reactor in vivo. ACS Synth Biol 2021;105:1087–94.
[24] Zhang Q, Wu Y-H, Huang X-S, Liu H-L, Wang Y. Design and optimization for efficient production of (S)-Canadine in Escherichia coli. ACS Sustainable Chem Eng 2024;1218:6941–51.
[25] Li Q, Sun B, Chen J, Zhang Y, Jiang Y, Yang S. A modified pCas/pTargetF system for CRISPR-Cas9-assisted genome editing in Escherichia coli. Acta Biochim Biophys Sin 2021;535:620–7.
[26] Moore SJ, Tosi T, Hleba YB, Bell D, Polizzi K, Freemont P. A cell-free synthetic biochemistry platform for raspberry ketone production. Cold Spring Harbor Laboratory; 2018.
[27] Forli S, Huey R, Pique ME, Sanner MF, Goodsell DS, Olson AJ. Computational protein-ligand docking and virtual drug screening with the AutoDock suite. Nat Protoc 2016;115:905–19.
[28] Reifenrath M, Boles E. Engineering of hydroxymandelate synthases and the aromatic amino acid pathway enables de novo biosynthesis of mandelic and 4-hydroxymandelic acid with Saccharomyces cerevisiae. Metab Eng 2018;45:246–54.
[29] Nakagawa A, Nakamura S, Matsumura E, Yashima Y, Takao M, Aburatani S, et al. Selection of the optimal tyrosine hydroxylation enzyme for (S)-reticuline production in Escherichia coli. Appl Microbiol Biotechnol 2021;10513:5433–47.
[30] Satoh Y, Tajima K, Munekata M, Keasling JD, Lee TS. Engineering of L-tyrosine oxidation in Escherichia coli and microbial production of hydroxytyrosol. Metab Eng 2012;146:603–10.
[31] Baltas M, Lapeyre C, Bedos-Belval F, Maturano M, Saint-Aguet P, Roussel L, et al. Kinetic and inhibition studies of cinnamoyl-CoA reductase 1 from Arabidopsis thaliana. Plant Physiol Biochem : PPB (Plant Physiol Biochem) 2005;438:746–53.
[32] Liu Q, Luo L, Zheng L. Lignins: biosynthesis and biological functions in plants. Int J Mol Sci 2018;192.
[33] Zou Y, Teng Y, Li J, Yan Y. Recent advances in the biosynthesis of coumarin and its derivatives. Green Chemical Engineering 2024;52:150–4.
[34] Roddan R, Ward JM, Keep NH, Hailes HC. Pictet-Spenglerases in alkaloid biosynthesis: future applications in biocatalysis. Curr Opin Chem Biol 2020;55:69–76.
[35] Nishihachijo M, Hirai Y, Kawano S, Nishiyama A, Minami H, Katayama T, et al. Asymmetric synthesis of tetrahydroisoquinolines by enzymatic Pictet-Spengler reaction. Biosci Biotechnol Biochem 2014;784:701–7.
[36] Jamil OK, Cravens A, Payne JT, Kim CY, Smolke CD. Biosynthesis of tetrahydropapaverine and semisynthesis of papaverine in yeast. Proc Natl Acad Sci U S A 2022;11933:e2205848119.
[37] Lv H, Zhang Y, Shao J, Liu H, Wang Y. Ferulic acid production by metabolically engineered Escherichia coli. Bioresources and bioprocessing 2021;81:70.
[38] Mansell DJ, Toogood HS, Waller J, Hughes JM, Levy CW, Gardiner JM, et al. Biocatalytic asymmetric alkene reduction: crystal structure and characterization of a double bond reductase from Nicotiana tabacum. ACS Catal 2013;33:370–9.
[39] Kim B, Binkley R, Kim HU, Lee SY. Metabolic engineering of Escherichia coli for the enhanced production of l-tyrosine. Biotechnol Bioeng 2018;11510:2554–64.
[40] Charles IG, Lamb HK, Pickard D, Dougan G, Hawkins AR. Isolation, characterization and nucleotide sequences of the aroC genes encoding chorismate synthase from Salmonella typhi and Escherichia coli. J Gen Microbiol 1990;1362:353–8.
[41] Hessing HG, van Rotterdam C, Pouwels PH. Expression of the Escherichia coli trpE gene in E. coli K12 bacteria: maximum level, rate and time of initiation of anthranilate synthetase production. Mol Gen Genet MGG 1987;2102:256–61.
[42] Kunjapur AM, Tarasova Y, Prather KL. Synthesis and accumulation of aromatic aldehydes in an engineered strain of Escherichia coli. J Am Chem Soc 2014;13633:11644–54.
[43] Prieto MA, Perez-Aranda A, Garcia JL. Characterization of an Escherichia coli aromatic hydroxylase with a broad substrate range. J Bacteriol 1993;1757:2162–7.
[44] Liebgott PP, Amouric A, Comte A, Tholozan JL, Lorquin J. Hydroxytyrosol from tyrosol using hydroxyphenylacetic acid-induced bacterial cultures and evidence of the role of 4-HPA 3-hydroxylase. Res Microbiol 2009;16010:757–66.
[45] Gibello A, Suárez M, Allende JL, Martín M. Molecular cloning and analysis of the genes encoding the 4-hydroxyphenylacetate hydroxylase from Klebsiella pneumoniae. Arch Microbiol 1997;1672–3:160–6.
[46] Chen W, Yao J, Meng J, Han W, Tao Y, Chen Y, et al. Promiscuous enzymatic activity-aided multiple-pathway network design for metabolic flux rearrangement in hydroxytyrosol biosynthesis. Nat Commun 2019;101:960.